Ground-state electric quadrupole moment of ^{31}Al

D. Nagae,[1,*] H. Ueno,[2,3] D. Kameda,[2] M. Takemura,[1] K. Asahi,[1] K. Takase,[1] A. Yoshimi,[2] T. Sugimoto,[2,†] K. Shimada,[1,‡] T. Nagatomo,[2] M. Uchida,[1] T. Arai,[1] T. Inoue,[1] S. Kagami,[1] N. Hatakeyama,[1] H. Kawamura,[3,§] K. Narita,[3] and J. Murata[3]

[1]*Department of Physics, Tokyo Institute of Technology, 2-12-1 Oh-okayama, Meguro-ku, Tokyo 152-8551, Japan*

[2]*RIKEN Nishina Center, 2-1 Hirosawa, Wako, Saitama 351-0198, Japan*

[3]*Department of Physics, Rikkyo University, 3-34-1 Nishi-Ikebukuro, Toshima-ku, Tokyo 171-8501, Japan*

(Received 16 October 2008; published 18 February 2009)

The ground-state electric quadrupole moment of ^{31}Al ($I^{\pi} = 5/2^{+}$, $T_{1/2} = 644(25)$ ms) has been measured by means of β-ray-detected nuclear magnetic resonance spectroscopy using a spin-polarized ^{31}Al beam produced in the projectile fragmentation reaction. The obtained Q moment, $|Q_{\rm exp}(^{31}{\rm Al})| = 112(32)\,e$ mb, is in agreement with conventional shell model calculations within the *sd* valence space. Previous results on the magnetic moment also support the validity of the *sd* model in this isotope, and thus it is concluded that ^{31}Al is located outside of the *island of inversion*.

DOI: 10.1103/PhysRevC.79.027301 PACS number(s): 21.10.Ky, 21.60.Cs, 27.30.+t, 29.27.Hj

The ground states of Ne, Na, and Mg isotopes with neutron numbers around the magic number $N = 20$ have been known to show anomalously tight bindings since the 1970s [1,2]. Later spectroscopic studies have revealed that the first exited 2^{+} levels are lowered [3,4] and their $B(E2)$ values are enhanced [5] sizably in these isotopes, and the possibility of deformation has been proposed. Theoretical analyses [6] have discussed the importance of 2p-2h excitations from the *sd* shell to the upper *pf* shell and concluded it is plausible that an inversion of amplitudes between the *sd* normal and the *pf* intruder configurations would lead to deformation of the ground states. The region of nuclei where such a phenomenon occurs is called the *island of inversion*. In elucidating the underlying mechanism for the inversion, the measurements of the electromagnetic moments have played an important role. For example in a series of neutron-rich Na isotopes, it has been found that, once entering the island of inversion, the ground-state magnetic dipole moment μ and electric quadrupole moment Q [7,8] show clear deviations from the conventional shell model predictions [9], indicating that μ and Q are sensitive to changes in the nuclear configuration [10]. Also in the recent study of Mg isotopes, anomalous ground-state properties have been revealed through the μ-moment measurements [11,12].

In the present work, the ground-state Q moment of ^{31}Al ($I^{\pi} = 5/2^{+}$, $T_{1/2} = 644(25)$ ms) has been measured by means of β-ray-detected nuclear magnetic resonance (β-NMR) spectroscopy [13] applied on a projectile fragment ^{31}Al implanted in an α-Al_2O_3 (corundum) single crystal in which a nonzero electric field gradient acts. A spin-polarized radioactive-isotope beam (RIB) of ^{31}Al was obtained from the projectile fragmentation reaction [14]. Because the neutron-rich aluminum isotopes are located in the neighborhood of the island of inversion, their electromagnetic moments would signify the possible onset of evolution in the nuclear structure that ultimately leads to the *inversion* phenomenon. So far, the μ moments of $^{31-34}$Al [15,16] and ^{30,32}Al [17] have been reported. The obtained values of μ for $^{30-32}$Al seem to stay within the conventional *sd* model predictions [9,18], indicating that their structures are suitably described within the normal *sd* model space. Those of ^{33,34}Al having neutron numbers $N = 20$ and 21, on the other hand, seem to indicate deviations from the $0\hbar\omega$ shell model predictions [16,19]. Because the island of inversion is considered to involve the nuclear deformation, the Q moment would be a more suitable probe. It has been found in a recent measurement that ^{32}Al has a very small Q moment, $|Q_{\rm exp}(^{32}{\rm Al})| = 24(2)\,e$ mb [20], characteristic of a simple $(\pi d_{5/2}{}^{-1} \otimes \nu d_{3/2}{}^{-1})^{J=1}$ configuration, indicating a spherical shape. The Q moment of ^{31}Al is important in elucidating how the nuclear shape evolves along the aluminum isotopes toward and beyond the ^{32}Al nuclide.

The experiment was carried out using the RIKEN projectile fragment separator RIPS [21]. The arrangement of RIPS for producing the spin-polarized RIB is essentially the same as that described in Ref. [20]. A beam of ^{31}Al was obtained from the fragmentation of ^{40}Ar projectiles at $E = 95\ A$ MeV on a 0.37 g/cm^2 thick ^{93}Nb target. It has been revealed that a spin-polarized RIB is obtained in the projectile fragmentation reaction simply by selecting the angle and momentum of the outgoing fragments [14]. Thus, ^{31}Al fragments emitted at angles $\theta_{\rm Lab.} = 1.3$–5.7° from the primary beam direction were accepted by RIPS using a beam swinger installed upstream of the target. Also, a range of momenta $p = 1.01$–$1.07 p_0$ was selected with a slit placed at the momentum-dispersive intermediate focal plane. Here $p_0 = 12.2$ GeV/c is the fragment momentum corresponding to the projectile velocity. The momentum distribution of ^{31}Al, though not measured at this time, is presumed to have a peak at around p_0 with a width $\Delta p \sim 0.06\ p_0$ (FWHM) that was obtained by considering an intrinsic width $\Delta p_{\rm Goldhaber} \approx 0.55$ GeV/c from the Goldhaber

*Present address: Japan Atomic Energy Agency, Tokai-mura, Ibaraki 319-1195, Japan; nagae.daisuke@jaea.go.jp

†Present address: Japan Synchrotron Radiation Research Institute (JASRI/SPring-8), 1-1-1 Kouto, Sayo, Hyogo 679-5198, Japan.

‡Present address: Cyclotron and Radioisotope Center, Tohoku University, 6-3 Aoba, Aramaki, Aoba-ku, Sendai, Miyagi 980-8578, Japan.

§Also at RIKEN Nishina Center, 2-1 Hirosawa, Wako, Saitama 351-0198, Japan.

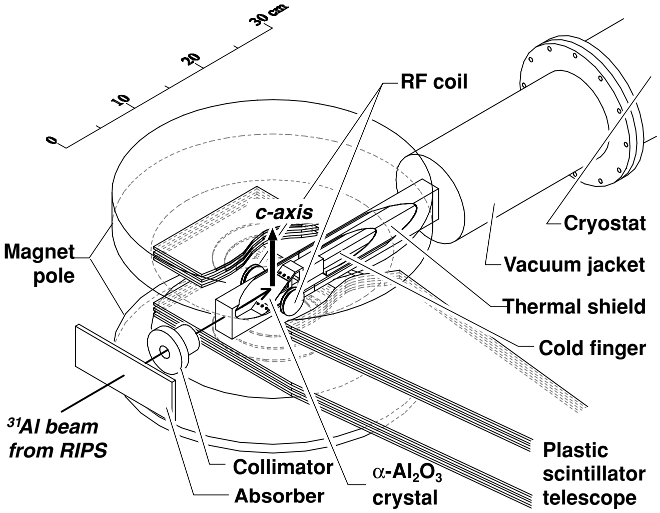

FIG. 1. Schematic layout of the β-NMR apparatus.

model [22] and the broadening effect $\Delta p_{\text{target}} \approx 0.40$ GeV/c due to a finite target thickness. The isotope separation was provided by combined analyses of the magnetic rigidity and momentum loss in the wedge-shaped degrader [21]. Then, the spin-polarized ^{31}Al nucleus was transported to a β-NMR apparatus located at the final focus of RIPS and implanted in a stopper of α-Al$_2$O$_3$ single crystal of hexagonal structure. A static magnetic field $B_0 = 501.768(3)$ mT was applied to the stopper. The layout of the β-NMR apparatus is shown in Fig. 1. The α-Al$_2$O$_3$ crystal was cut into a $18 \times 32 \times 0.6$ mm slab and was mounted in a stopper chamber so that the c axis was oriented parallel to the B_0 field. The stopper was kept in vacuum and cooled to a temperature $T = 70 \sim 100\ K$ to suppress the spin-lattice relaxation of ^{31}Al during the β decay. The spin-lattice relaxation time T_1 at $T = 100\ K$ was evaluated to be $T_1 \approx 4.5\ s$, based on the measured T_1 for ^{27}Al in α-Al$_2$O$_3$ at room temperature [23,24] and the $T_1 T^2 Q^2 =$ const. law [25].

The Q moment interacts with an electric field gradient eq acting at the site of the implanted nucleus in a single crystal stopper. The eqQ interaction causes the energy shift in the individual Zeeman magnetic sublevels. Thus, the Q moment is determined from the measurement of the frequencies for the resonance transition between the Zeeman + quadrupole splitted sublevels, whose signal is detected as a change in the β-ray asymmetry (the β-NQR method). The β rays emitted from the implanted nucleus were detected with scintillator telescopes located above and below the stopper, each consisting of three 1-mm-thick plastic scintillators. The up/down ratio R of the β-ray counts is written as

$$R = a\frac{1 + v/c \cdot A_\beta P}{1 - v/c \cdot A_\beta P} \simeq a(1 + 2A_\beta P), \qquad (1)$$

where a is a constant factor representing asymmetries in the counter solid angles ($\Omega_\beta \approx 4\pi \times 0.26$ sr each) and efficiencies, v/c the velocity of the β particle, A_β the asymmetry parameter, and P the ^{31}Al nuclear spin polarization. The β rays lose energies of 960 keV on average upon penetrating the stopper material and a wall of the vacuum jacket and then deposit about 260 keV in each of the three scintillators. The threshold energy for the β-ray detection in triple coincidence among the three scintillators is evaluated [26] to be 1740 keV, and the detection efficiency including the energy threshold and the detection solid angle is about 29% for the β rays from ^{31}Al, for which the experimentally known major branches are to the $3/2^+$ ground state of ^{31}Si (65%, $Q_\beta = 7995$ keV), to the $3/2^+$2317-keV state (26%), to the $5/2^+$1695-keV state (8%), and to the $1/2^+$752-keV state (1%) [27]. Because only the $E_\beta \gtrsim$ 1500 keV (or $v/c \gtrsim 0.97$) portion of the spectrum was detected, the ratio R in Eq. (1) is well approximated by the second expression by simply setting $v/c \approx 1$. The adiabatic fast passage (AFP) technique [28] was incorporated to pursue the reversal, but not the destruction, of the spin polarization. By taking a double ratio R/R_0, where R_0 is the value for R measured without an oscillating magnetic field B_1, the resonance frequency is derived from the position of a peak or dip deviating from unity. The measurements were carried out in the following sequence. The beam was pulsed with beam-on and bean-off periods of 1 and 1.126 s, respectively. In the beam-off period of a beam cycle, the B_1 field was applied for the first 63 ms duration. Then, the β rays were counted for 1 s, and in the last 63 ms of the the beam-off period the B_1 field was applied again to restore the spin direction so that the ratio R in the succeeding cycle might not be affected by the surviving activities. Such beam cycles were executed with n different sets of frequencies as described below and then with the B_1 field interrupted (the R_0 measurement). These $n + 1$ beam cycles were repeated until the sufficient measurement statistics were attained. By inserting the R_0 measurement in this way, the effect of long-term fluctuations in, e.g., the beam profile at the target should be removed. The B_1 field was applied in a direction perpendicular to the external field B_0 with a pair of coils located outside a vacuum jacket, in which the α-Al$_2$O$_3$ stopper was placed. In a first order perturbation theory, the resonance frequency $\nu_{m,m+1}$ between magnetic sublevels m and $m + 1$ of the spin I under the combined Zeeman and quadrupole interactions is given by

$$\nu_{m,m+1} = \nu_{\text{L}} - \nu_{\text{Q}} \cdot (3\cos^2\theta_{c\ \text{axis}} - 1)\frac{3(2m + 1)}{8I(2I - 1)}, \qquad (2)$$

where ν_L denotes the Larmor frequency, $\nu_Q = eqQ/h$ the quadrupole coupling constant, eq the electric field gradient along the c axis (the additional term arising from a deviation η from the axial symmetry of the field gradient tensor is omitted, because η is reported to be small [29]), and $\theta_{c\,\text{axis}}$ the angle between the c axis and the B_0 field. Q and h denote the Q moment and the Planck's constant, respectively. Inserting $I = 5/2$ and $\theta_{c\,\text{axis}} = 0$ for the present ^{31}Al experiment, Eq. (2) reads as

$$\nu_{m,m+1}(\nu_Q) = \nu_L - \frac{3}{40}(2m + 1)\nu_Q \qquad (3)$$

$$= \begin{cases} \nu_L + (3/10)\nu_Q & \text{for} \quad (m, m+1) = (-5/2, -3/2); \\ & \quad (\text{frequency "}a\text{"}) \\ \nu_L + (3/20)\nu_Q & \text{for} \quad (-3/2, -1/2), (\text{"}b\text{"}) \\ \nu_L & \text{for} \quad (-1/2, +1/2), (\text{"}c\text{"}) \\ \nu_L - (3/20)\nu_Q & \text{for} \quad (+1/2, +3/2), (\text{"}d\text{"}) \\ \nu_L - (3/10)\nu_Q & \text{for} \quad (+3/2, +5/2), (\text{"}e\text{"}). \end{cases} \qquad (4)$$

Once the true value for ν_Q is inserted, sweeping the B_1 field across $\nu_{m,m+1}(\nu_Q)$ leads to a reversal of population between sublevels m and $m+1$ (the adiabatic fast passage technique). Note that the full reversal of spin, $+5/2 \leftrightarrow -5/2, +3/2 \leftrightarrow -3/2, +1/2 \leftrightarrow -1/2$, requires a sequence of stepwise reversals between two contiguous sublevels [30]. The B_1 field was applied in $I(2I+1) = 15$ steps in a sequence *abcdeabcdabcaba* within the B_1 application period of 63 ms duration. In each step the frequency ν was swept from $\nu_{m,m+1}(\nu_Q{}^{\text{lower}})$ to $\nu_{m,m+1}(\nu_Q{}^{\text{upper}})$ with $\nu_Q{}^{\text{lower}}$ and $\nu_Q{}^{\text{upper}}$ denoting the lower and upper bounds of the searched ν_Q region. Prior to the present Q-moment measurement, a β-NMR experiment was carried out on ^{31}Al in a Si crystal using the same apparatus and B_0 setting. The obtained magnetic moment $|\mu(^{31}\text{Al})| = 3.824(8)\ \mu_N$ is in good agreement with the previously reported values [15,16]. For the Larmor frequency ν_L in Eq. (3), we adopted a value $\nu_L = 5850(12)$ kHz obtained from this measurement.

Thus, the β-ray count ratio R/R_0 is expected to differ from unity when the B_1 field sequence is executed for the ν_Q region that includes the true ν_Q value. Figure 2 shows the measured R/R_0 ratio for ^{31}Al in α-Al_2O_3 as a function of ν_Q (the β-NQR spectrum). The horizontal bar attached to the data point (solid circle) indicates the ν_Q region over which the B_1 field frequency was swept. The vertical bar represents the error in R/R_0 arising from the β-ray counting statistics. The R/R_0 value at the dip bottom shows a displacement of 5.3 standard deviation from unity, clearly indicating the occurrence of the AFP spin reversal. The width of the dip, however, appears to be substantially broader than a calculated width 653 kHz (FWHM) for the present AFP sweep width (see horizontal bars attached to the data points in Fig. 2). Although an externally implanted Al ion would be most likely to stop at the site of the same element in the host crystal, there may be a possibility that some portion of the implanted ions stop at other, metastable sites. Also, there might be another case where the implanted ions stop at the site of ^{27}Al in α-Al_2O_3 but some of them

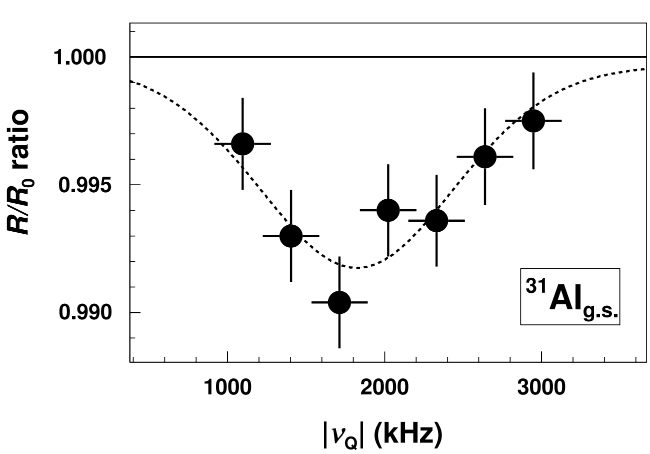

FIG. 2. A NQR spectrum obtained in an α-Al_2O_3 crystal for the ground state of ^{31}Al. The R/R_0 ratio is plotted as a function of ν_Q. The vertical bar attached to the data point represents the statistical error due to β-counting statistics, while the horizontal bar indicates the width of ν_Q frequency sweep. The result of the least-χ^2 fitting analysis is shown by a dotted curve.

are accompanied by a near-by lattice defect produced by the implantation, thus leading to a shifted NQR resonance. In these cases the NQR spectrum would show a broadened dip.

The obtained NQR spectrum was fitted with a function,

$$F(\nu_Q) = a \int G_\sigma(\xi) \cdot \mathcal{F}_{\text{AFP}}(\nu_Q - \nu_Q{}^{(0)} - \xi)\, d\xi + b, \qquad (5)$$

with four free parameters $\nu_Q{}^{(0)}$, σ, a, and b to be determined through the fitting. The $F(\nu_Q)$ function is a Gaussian convolution of a theoretical shape function $\mathcal{F}_{\text{AFP}}(x)$ of a detuning x (i.e., $f(x)$ of Eq. (4) in Ref. [31]). The parameter $\nu_Q{}^{(0)}$ represents the position of the dip, from which the quadrupole coupling constant eqQ/h will be deduced. The parameter σ is the width of the Gaussian function $G_\sigma(\xi) \equiv (\sqrt{2\pi}\sigma)^{-1}\exp(-\xi^2/2\sigma^2)$, representing extrabroadening effects that are not included in the function $\mathcal{F}_{\text{AFP}}(x)$. Extrabroadening may arise from distribution of the eq value due to lattice defects or impurities in the stopper crystal and misalignments in the c-axis orientation and ν_L setting. In the present analysis such effects are expressed as a finite value of σ. The extrabroadening was not included in the preliminary reports [30,32].

From the fitting analysis of the NQR spectrum, we obtained $\nu_Q{}^{(0)} = 1824(119)$ kHz for the dip position. The resulting curve $F(\nu_Q)$ is shown in Fig. 2 by a dotted line. Although the parameter $\nu_Q{}^{(0)}$ is determined with a rather small uncertainty ($\delta^{\text{fit}}\nu_Q{}^{(0)} = 119$ kHz) from the fitting procedure, the actual spectrum is dominated by a much larger broadening, $\sigma = 506$ kHz, whose origins are not well pinpointed, as discussed above. We therefore take into account the extra width σ as an independent error and assign an experimental error $\delta\nu_Q{}^{(0)} = 520$ kHz, as shown in Table I. As a result, we obtain a quadrupole coupling constant $|\nu_Q| = |eqQ/h| = 1824(520)$ kHz. The Q moment of ^{31}Al is deduced from the relation $|Q(^{31}\text{Al})| = |Q(^{27}\text{Al}) \cdot \nu_Q(^{31}\text{Al})/\nu_Q(^{27}\text{Al})|$, where $Q(^{27}\text{Al})$ and $\nu_Q(^{27}\text{Al})$ denote the Q moment of ^{27}Al and the quadrupole coupling constant of ^{27}Al in α-Al_2O_3, respectively. By inserting the recently reported Q moment $Q(^{27}\text{Al}) = 146.6(10)\,e$ mb [33] and quadrupole coupling constant $\nu_Q(^{27}\text{Al}) = 2389(2)$ kHz [34], the ground-state Q moment ^{31}Al is determined as $|Q_{\text{exp}}(^{31}\text{Al})| = 112(32)\,e$ mb.

In Fig. 3, the experimentally known Q moments for the neutron-rich aluminum isotopes [20,33,35] including the

TABLE I. Uncertainties taken into account for the determination of the $|Q_{\text{exp}}(^{31}\text{Al})|$ moment. Those uncertainties were converted into the corresponding ν_Q frequencies.

Resonance ν_Q	1824 kHz
Statistical error	
Fitting error	119 kHz
Systematic errors	
Ambiguity from the resonance width	506 kHz
Uncertainty of the electric field gradient	13 kHz
Ambiguity of the θ_{caxis}-angle setting	0.9 kHz
Total	520 kHz
$\rightarrow |Q_{\text{exp}}(^{31}\text{Al})|$	$112 \pm 32\,e$ mb

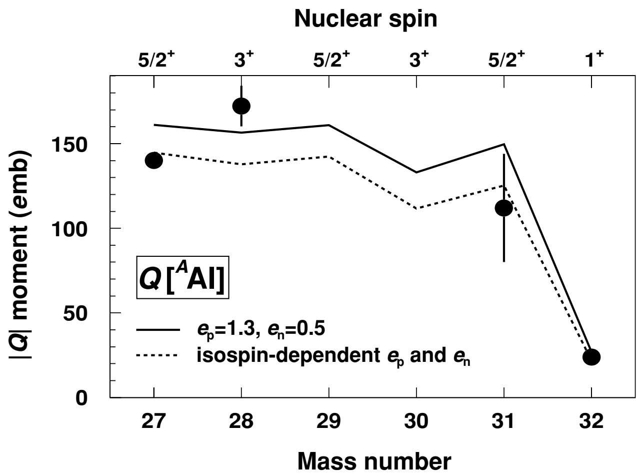

FIG. 3. Experimental (solid circle) and theoretical (solid and dotted lines) Q moments of neutron-rich aluminum isotopes as a function of mass number; nuclear spins are also shown. Theoretical values are obtained from shell model calculations within the sd shell with the USD interaction, using the constant effective charges $e_p = 1.3$ and $e_n = 0.5$ (solid line) and isospin-dependent effective charges [31] (dotted line).

present data are plotted as a function of the mass number A. Also, the results of shell model calculations within the sd shell [9,18] are shown by the solid line. The calculations reproduce the observed trend of the Q moments in the $^{27-32}$Al region fairly well: $|Q_{\rm exp}|$ stays almost constant at $|Q_{\rm exp}| \sim 150\,e$ mb, but suddenly decreases to a very small value at $A = 32$ [20]. These calculations have employed effective charges $e_p = 1.3$ for protons and $e_n = 0.5$ for neutrons. One could include the effect of isospin dependence of the effective charges, which had been pointed out in Ref. [36] and was observed experimentally for the first time in the Q moments of boron isotopes [31]. The dotted line shows the calculated Q with the effective charges varied with isospin according to the expression given in Ref. [31]. The use of the isospin-dependent e_p and e_n reduces the calculated Q by $10 \sim 15\%$ in the $^{27-32}$Al isotopes and improves the agreement particularly in the ^{31}Al Q moment, although the experimental error in $Q(^{31}\text{Al})$ is not small. Finally, in contrast to the approximate accordance of the sd shell calculations with experiment, an anticipation that the deformation might set in somewhere along the chain of Al isotopes proves to be not the case at least until $A = 32$, because sizes of the experimental Q presented in Fig. 3 are much smaller than those expected for deformations of $\beta \sim 0.5$ occurring in the neighboring nucleus ^{30}Mg [37].

In summary, the ground-state Q moment of ^{31}Al has been determined by the β-NQR method, using the fragmentation-induced spin polarization. The obtained Q for ^{31}Al as well as known $|Q|$ values for other neutron-rich aluminum isotopes were found to be well explained by shell model calculations within the sd shell. Because the magnetic moment of ^{31}Al recently determined [15,16] is explained with the same calculations, it is concluded that ^{31}Al is located outside the island of inversion.

The authors thank the staff of the RIKEN Ring Cyclotron for their support during the experiment. They thank Dr. E. Yagi for useful help and advice with the X-ray diffraction analysis of the α-Al_2O_3 sample. The authors D.N. and K.S. are grateful for the Junior Research Associate Program in RIKEN. This experiment was carried out at the RI Beam Factory operated by RIKEN Nishina Center and CNS, University of Tokyo, under Experimental Program R398n(5B).

[1] C. Thibault *et al.*, Phys. Rev. C **12**, 644 (1975).
[2] C. Détraz *et al.*, Nucl. Phys. **A394**, 378 (1983).
[3] C. Détraz *et al.*, Phys. Rev. C **19**, 164 (1979).
[4] D. Guillemaud *et al.*, Nucl. Phys. **A426**, 37 (1984).
[5] T. Motobayashi *et al.*, Phys. Lett. **B346**, 9 (1995).
[6] E. K. Warburton, J. A. Becker, and B. A. Brown, Phys. Rev. C **41**, 1147 (1990).
[7] G. Huber *et al.*, Phys. Rev. C **18**, 2342 (1978).
[8] M. Keim *et al.*, Eur. Phys. J. A **8**, 31 (2000).
[9] B. H. Wildenthal, Prog. Part. Nucl. Phys. **11**, 5 (1984).
[10] Y. Utsuno, T. Otsuka, T. Glasmacher, T. Mizusaki, and M. Honma, Phys. Rev. C **70**, 044307 (2004).
[11] G. Neyens *et al.*, Phys. Rev. Lett. **94**, 022501 (2005).
[12] D. T. Yordanov *et al.*, Phys. Rev. Lett. **99**, 212501 (2007).
[13] K. Sugimoto, A. Mizouchi, K. Nakai, and K. Matsuta, J. Phys. Soc. Jpn. **21**, 213 (1966).
[14] K. Asahi *et al.*, Phys. Lett. **B251**, 488 (1990); H. Okuno *et al.*, *ibid.* **B335**, 29 (1994).
[15] D. Borremans *et al.*, Phys. Lett. **B537**, 45 (2002).
[16] P. Himpe *et al.*, Phys. Lett. **B643**, 257 (2006).
[17] H. Ueno *et al.*, Phys. Lett. **B615**, 186 (2005).
[18] B. A. Brown, A. Etchegoyen, and W. D. M. Rae, OXBASH, MSU Cyclotron Laboratory Report No. 524, 1986.
[19] P. Himpe *et al.*, Phys. Lett. **B658**, 203 (2008).
[20] D. Kameda *et al.*, Phys. Lett. **B647**, 93 (2007).
[21] T. Kubo *et al.*, Nucl. Instrum. Methods B **70**, 309 (1992).
[22] A. S. Goldhaber, Phys. Lett. **B53**, 306 (1974).
[23] E. R. Andrew and D. P. Tunstall, Proc. Phys. Soc. (London) **78**, 1 (1961).
[24] A. P. M. Kentgens *et al.*, Solid State Nucl. Magn. Reson. **3**, 315 (1994).
[25] R. L. Mieher, Phys. Rev. Lett. **4**, 57 (1960).
[26] R. Brun and F. Carminati, CERN Application Software Group, GEANT3.2, CERN Program Library Writeup Report No. W5013, 1994.
[27] P. M. Endt and R. B. Firestone, Nucl. Phys. **A633**, 1 (1998).
[28] A. Abragam, *The Principle of Nuclear Magnetism* (Clarendon, Oxford, 1961).
[29] A. J. Woo, Bull. Korean Chem. Soc. **20**, 1205 (1999).
[30] D. Nagae *et al.*, Nucl. Instrum. Methods B **266**, 4612 (2008).
[31] H. Ogawa *et al.*, Phys. Rev. C **67**, 064308 (2003).
[32] H. Ueno *et al.*, Eur. Phys. J. Special Topics **150**, 185 (2007).
[33] V. Kellö *et al.*, Chem. Phys. Lett. **304**, 414 (1999).
[34] S. J. Gravina and P. J. Bray, J. Magn. Reson. **89**, 515 (1990).
[35] H.-J. Stöckmann *et al.*, Hyp. Int. **4**, 170 (1978).
[36] A. Bohr and B. R. Mottelson, *Nuclear Structure* (World Scientific, Singapore, 1998), Vol. II.
[37] V. Chisté *et al.*, Phys. Lett. **B514**, 233 (2001).